TECHNISCHE MECHANIK
an open access journal

journal homepage: www.ovgu.de/techmech

Tech. Mech., Vol. 44, Is. 3, (2024), 181–193

Received: 30.08.2024
Accepted: 13.02.2025
Available online: 14.02.2025

Identifying acoustic coefficients of sound insulation panels: A novel predictive approach

Mahmoud B. Elmokadem [1], S. Abolfazl Zahedi [2⋆], Khaled Laib [3], and Vadim V. Silberschmidt [2]

[1] *School of Engineering and Sustainable Development, De Montfort University, UK*
[2] *Wolfson School of Mechanical, Electrical and Manufacturing Engineering, Loughborough University, UK*
[3] *School of Engineering, University of Leicester, UK*

Abstract: This research introduces a novel predictive approach for estimating the acoustic coefficients of sound insulation materials, aiming to enhance both the accuracy and efficiency of acoustic performance assessments. The proposed method addresses the limitations of traditional testing techniques, which are often costly and labour-intensive by offering a fast-prototyping tool for acoustics engineers. The algorithm integrates fuzzy logic with a high-resolution microscope image analysis to predict key acoustic parameters, including absorption coefficient rate. The algorithm achieved a high predictive accuracy by being trained on a diverse dataset of material properties and validated against experimental laboratory results. This approach provides a cost-effective and reliable alternative to conventional testing methods, enabling rapid evaluation of material performance while maintaining precision.

Keywords: Acoustic Coefficient, System Identification, Sound Insulation, Predictive Approach, Material Characterisation.

1 Introduction

Sound insulation materials are crucial in controlling noise pollution, improving privacy, and creating comfortable environments in residential, commercial, and industrial settings. With the increasing demand for effective sound insulation solutions, accurate assessment of acoustic performance has become a priority for acoustics engineers and materials scientists. Traditional methods for measuring acoustic properties, e.g., sound transmission loss and absorption coefficients, often involve extensive laboratory tests using tools such as acoustic impedance tubes or anechoic chambers. The acoustic impedance tube is a widely accepted device used to measure the acoustic properties of materials Hiremath et al. (2021). It employs the principle of standing wave ratios to determine the sound absorption coefficients and transmission loss by analysing the pressure fluctuations of sound waves within a cylindrical tube. This method allows for the assessment of sound insulation materials at specific frequencies, providing precise data on their performance. However, using the impedance tube requires careful sample preparation and can only assess one dimension of the acoustic behaviour of a material at a time. This limitation can lead to an incomplete understanding of the performance of the material in real-world scenarios. On the other hand, the anechoic chamber is designed to eliminate reflections and external noise, providing a controlled space to test the propagation properties of acoustic waves in materials Nash (2019). These chambers allow a comprehensive evaluation of the sound insulation performance in a range of frequencies and conditions. The results obtained with anechoic chambers are highly accurate, making them ideal for research and development. However, the construction and maintenance of these chambers can be prohibitively expensive, and the time required to conduct experiments in such settings can be significant.

While effective, acoustic impedance tubes and anechoic chamber approaches are costly, labour intensive, and time-consuming. This accelerated the development of more efficient and reliable assessment techniques. In recent years, advances in machine learning and data analysis have opened new avenues to predict the acoustic performance of materials. However, many existing approaches focus mainly on empirical methods Mak and Wang (2015), or artificial neural networks based on empirical methods Aliabadi et al. (2014), or simple linear models Vorländer (2006) that predict basic parameters of the material, such as mass, density, and stiffness. Such models might not capture the complexity inherent in the behaviour of acoustic materials. Consequently, there is a pressing need for novel predictive techniques that can accurately estimate the acoustic coefficients of sound insulation. Materials are based on their properties, ultimately optimising the design and selection process. This paper introduces a predictive algorithm that leverages fuzzy logic techniques and image analysis algorithms to predict the effective acoustic parameters, especially the absorption rate, for a medium-low frequency range (200 to 1600 Hz).

The primary objectives of this study are twofold first, to determine whether a predictive model trained on a cross-material dataset can generalise effectively without relying on material-specific data, and second, to evaluate whether small, individualised datasets are sufficient for training an accurate predictive model. By exploring these questions, this study aims to develop a reliable and efficient tool for acoustics engineers, enabling them to evaluate and optimise sound insulation materials effectively.

⋆ E-mail address: A.Zahedi@lboro.ac.uk
doi: 10.24352/UB.OVGU-2024-065

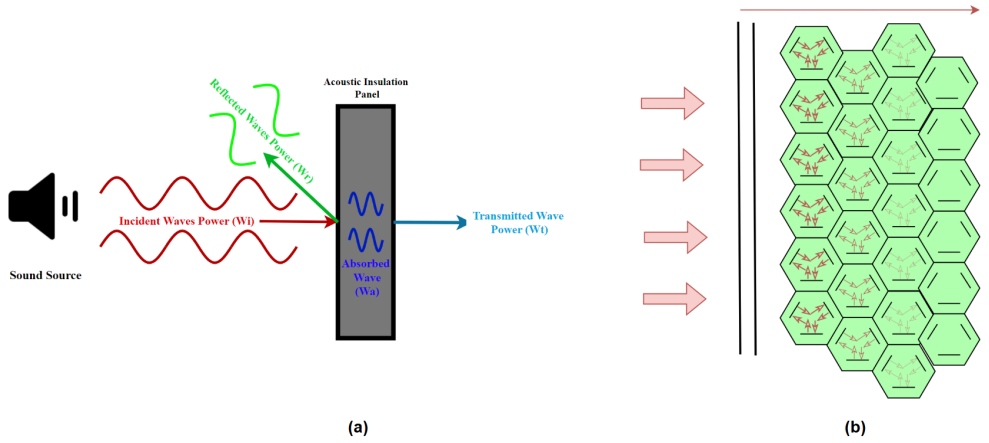

Fig. 1: a) Sound propagation in insulation panels b) Sound-wave penetration in pours materials.

Paper contributions:
The main contributions of this paper can be summarised as follows:

- Innovative predictive method: Introduces a novel approach for predicting the acoustic coefficients of sound insulation panels, combining fuzzy logic and image analysis algorithms.
- Efficient and cost-effective solution: Develops an algorithm that provides a more efficient and cost-effective alternative to traditional experimental methods for predicting sound absorption coefficients.
- Leverage of microscopic properties: Utilises microscopic structural properties to enable rapid and reliable assessments of overall acoustic performance.
- High consistency across samples: Demonstrates the algorithm reliability, maintaining prediction errors within an acceptable range across various material samples.

Paper outline: This paper is organised as follows. Section 2 presents general aspects of acoustic wave propagation and the factors impacting this propagation that are subsequently exploited to derive our main results. Section 3 presents the proposed algorithm to predict acoustic parameters. Section 4 is dedicated to presenting and discussing our results, whilst conclusions are drawn in Section 5.

2 Principles of acoustic wave propagation

2.1 Acoustic insulation parameters

In contrast to electromagnetic waves that can propagate without a medium, the sound waves rely on disturbance within a medium, classifying it as a mechanical wave that disturbs the medium to be transferred from the source to the receiver. This is caused by the acoustic energy that works by periodically displacing air, resulting in cyclic changes in air pressure Bies et al. (2017). The sound pressure wave refers to a zone where pressure variations travel through a medium. The sound pressure wave is defined by its frequency and amplitude, where the frequency refers to the number of pressure cycles per second, whilst the amplitude measures the strength (or intensity) of such pressure variations. In the context of sound insulation, three key terms frequently arise: transmission loss, absorption rate, and reflection rate. Fig. 1 (a) illustrates the interaction of an incident sound wave with a sound insulation panel.
According to the principles of energy conservation law Thorby (2008), the incident wave (W_i) is divided into three components: the absorbed wave (W_a), the reflected wave (W_r), and the transmitted wave (W_t). This relationship can be mathematically expressed as follows:

$$W_i = W_r + W_a + W_t. \tag{1}$$

Each component represents a different aspect of the sound wave interaction with the material. The reflected wave (W_r) represents the part of the sound wave that reflected back from the surface of the material Höpe (2014).
The reflection coefficient (R) is defined as the ratio of the reflected sound energy (W_r), to the incident sound energy (W_i). The amount of a wave reflected back into the incident medium (R) is determined by the characteristic impedance (Z) of each medium. The characteristic impedance, which represents the resistance to wave propagation, is calculated by multiplying the speed of the sound wave (c) by the density of the medium (ρ). The reflection coefficient (R) depends on the difference in the characteristic impedance between the two mediums Keefe et al. (1992). A greater impedance mismatch results in higher reflection, whereas a smaller impedance allows more of the wave to be transmitted into the second medium.

$$R = \frac{W_r}{W_i} = \left(\frac{Z_2 - Z_1}{Z_2 + Z_1}\right)^2 = \left(\frac{\rho_2 c_2 - \rho_1 c_1}{\rho_2 c_2 + \rho_1 c_1}\right)^2. \tag{2}$$

The sound absorption coefficient α represents the most appropriate parameter to characterise the sound absorption properties of materials. It is defined as the ratio of the sound energy absorbed (W_a) by a surface to the total sound energy incident upon it (W_i), with values ranging from 0 to 1. The sound absorption coefficient depends on the angle of incidence. However, when the incident sound field is diffuse, it is typically assumed that sound waves approach the surface with equal probability from all directions Hopkins (2012), given as follows Peng (2017):

$$\alpha = \frac{W_a}{W_i} \tag{3}$$

The sound transmission loss (STL) quantifies the difference in sound energy levels between the incident sound on one side of a barrier and the transmitted sound on the other side. STL indicates how effective a material is at blocking or attenuating sound. Higher STL values correspond to greater sound attenuation, making the material more effective at soundproofing. It is defined as the ratio of the incident acoustic power on a material to the transmitted power[1] through it Kim (2010):

$$\mathrm{STL} = \frac{W_i}{W_t} = (1 - R)^{-1}\,, \tag{4}$$

and is expressed in decibels (dB) as

$$\mathrm{STL\ (dB)} = -10 \log_{10} (1 - R)\,. \tag{5}$$

There are two primary standards for measuring the acoustical properties of materials using a standing wave tube commonly referred to as (*Kundt′stube*): ISO 10534-2 Int (2002) and its American counterparts: (i) ASTM E1050-12 AST (2012) and (ii) ASTM E2611-17 AST (2017). Both standards utilise the tube's capabilities to provide precise acoustic measurements under controlled conditions by capturing sound pressure at various points to calculate surface impedance—a critical parameter that determined sound interacts with a material, including absorption, reflection, and transmission. For absorption measurements (ISO 10534-2/ASTM E1050-12), the reflection coefficient is directly linked to material impedance; materials with surface impedance close to the characteristic impedance of air exhibit minimal reflection and high absorption, while those with significant impedance mismatches reflect more sound and absorb less Zhang et al. (2014); Arunkumar and Jeyanthi (2017). For transmission-loss measurements (ASTM E2611-17), STL is influenced by the impedance contrast between the material and the surrounding medium, with high-impedance materials effectively blocking or attenuating sound transmission by limiting the energy that passes through them. Compared to parallel-room methods, such as those described in ISO 354 Int (2015) and ISO 10140-2 Int (2010), the standing-wave tube offers a more direct and efficient approach, requiring less space and smaller samples and being less affected by background noise, enabling precise evaluations of impedance characteristics and their impact on acoustic performance. While the foundational equations 1 - 5 discussed above provide a theoretical basis for these interactions, our proposed method does not rely on them. Instead, it employs a fuzzy logic engine and image analysis to directly predict the average sound absorption rate over a defined frequency range, offering a cost-effective alternative to conventional methods that require expensive data acquisition systems and measurement microphones.

2.2 Effect of material characteristics on acoustic absorption efficiency

The internal structure of porous materials significantly influences their acoustic absorption properties Maria et al. (2011). In non-porous materials, incident sound energy is primarily reflected, resulting in minimal absorption. In contrast, highly porous materials facilitate deep penetration of pressure waves, leading to multiple internal reflections inside the pores. These interactions with the solid framework generate frictional losses, converting acoustic energy into heat thereby enhancing absorption efficiency. This phenomenon is particularly evident in materials such as glass fibres, polymers, and metal foams. For optimal absorption, the pressure wave must penetrate sufficiently to mitigate immediate reflection, as illustrated in Fig. 1(b).

Porosity alone, however, does not guarantee effective acoustic insulation. The absorption efficiency depends on the relationship between the mean free path of air molecules and the spacing between the pore walls. When pore sizes are too small or poorly interconnected, sound waves cannot penetrate deeply, causing even open-cell structures to behave like closed-cell materials in acoustic applications. For example, conventional aerogels, despite their extremely high porosity (typically 80–90%), exhibit limited sound absorption due to their nanoscale pore diameters (2–20 nm), which restrict wave penetration Shao et al. (2024).

In addition, material compression affects the acoustic absorption properties. Castagnède et al. (2000) found that compressing a homogeneous porous layer reduces porosity and characteristic length while increasing tortuosity. However, the primary reason for the observed decrease in the absorption coefficient was the reduced thickness of the compressed material. Similar findings were reported in subsequent studies Allampalayam Jayaraman et al. (2005).

The presence of an air cavity behind an insulating material also influences absorption performance. Research by Hakamada et al. (2006) shows that an air gap between the material and a rigid backing surface enhances absorption by modifying the acoustic impedance and increasing the effective thickness of the absorbing layer. Interestingly, Aso and Kinoshita (1965) observed that for thin, highly porous samples, the maximum absorption coefficient decreases slightly as the air gap increases, while for thicker samples, absorption remains nearly constant regardless of the depth of the air gap.

In general, the acoustic performance of a material is intricately linked to its microscopic structure, including the size, shape, and distribution of its pores. When pore dimensions are comparable to the mean free path of air molecules, pressure waves are effectively trapped, leading to viscous and thermal energy dissipation Budtova et al. (2023). However, if the pores are too small, too large, or insufficiently interconnected, the effectiveness of the material as an acoustic absorber is significantly reduced. Thus, optimising the pore structure and material thickness is essential for achieving efficient sound absorption.

[1] Equations (4)-(5) assume that the absorbed wave (W_a) is negligible.

3 Proposed approach

In this section, a sound absorption prediction algorithm is introduced and tailored specifically for insulation panels, leveraging fuzzy logic theory as its computational framework. The algorithm aims to predict the sound absorption coefficient by accounting for key factors that influence acoustic performance, such as the material's porosity, density, thickness, pore size distribution, and excitation frequency.

3.1 Pore-size identification algorithm

The developed algorithm leverages image analysis for pore-size identification, as illustrated in Fig. 2. The process begins with the acquisition of high-resolution microstructure images, captured at a resolution of 25 μm using a high-resolution microscope, to enable detailed pore characterization, as shown in Fig. 2 (a). Preprocessing steps, such as contrast enhancement, are applied to improve the distinction between pores and the surrounding solid matrix. These images are then converted into enhanced grayscale versions, as depicted in Fig. 2 (b), to facilitate effective pore isolation during segmentation. The segmentation process partitions the image into distinct regions, differentiating pores from the material matrix based on intensity variations, as demonstrated in Fig. 2 (c). Advanced image-processing techniques, including thresholding and edge detection, are employed to achieve this differentiation. Morphological operations are subsequently applied to eliminate noise and refine pore boundaries, enhancing accuracy. To address challenges posed by overlapping or closely spaced pores, watershed segmentation is utilized, effectively separating merged pores during initial segmentation, as shown in Fig. 2 (d). the algorithm workflow is illustrated in Fig. 2 (e).

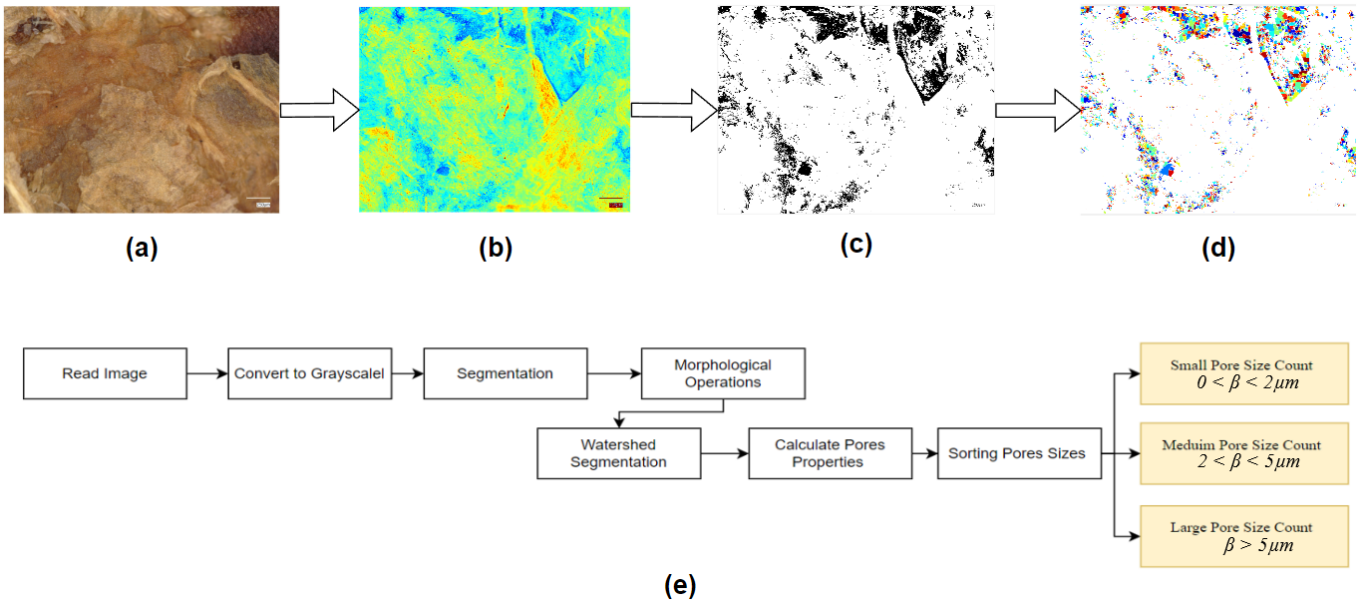

Fig. 2: (a) High resolution microscope Image of a coffee-chaff-based composite material. (b) Depth map, (c) Binary segmentation. (d) Pore space segmentation. (e) Workflow of image analysis and algorithm for pore size identification.

The main aim of this algorithm is to classify the pore sizes of composite base insulation materials to better understand their impact on acoustic performance.

The algorithm builds on existing methodologies for extraction of the pore network from micro-tomography images, as described in Aliabadi et al. (2014) and Rabbani et al. (2014). It employs a series of mathematical steps and operations to process images and obtain detailed pore size data.

The initial step involves converting the high-resolution microscopy images into greyscale to enhance the contrast between the pore regions and the surrounding material matrix. Greyscale conversion simplifies the image data by reducing it to intensity values, $H(i,j)$, which are calculated as $H(i,j) = 0.2989 \cdot R(i,j) + 0.5870 \cdot G(i,j) + 0.1140 \cdot B(i,j)$, where $R(i,j)$, $G(i,j)$, and $B(i,j)$ are the red, green, and blue pixel intensities, respectively. This conversion emphasises structural details critical for segmentation. Thereafter, to separate pores from the solid matrix, a thresholding technique is applied with the threshold T, generating a binary mask $B(i,j)$, which is equal to 1 if $H(i,j) \leq T$ and 0 otherwise. The threshold value T is determined adaptively using Otsu's method, ensuring optimal differentiation between pore and matrix regions.

Following this step, morphological operations are applied to the binary mask B to refine the segmentation by removing noise and enhancing the clarity of pore boundaries. These operations include dilation, which expands pore boundaries to fill the gaps, and erosion, which contracts the boundaries to eliminate small artefacts. A structuring element S is used to guide these transformations. Hereafter, watershed segmentation is applied for closely packed pores, to ensure each pore is treated as a separate entity. This method interprets the grayscale image as a 3D topographic surface, identifying regions by minimizing. $\int_\Omega |\nabla u| \, d\Omega$,where u is the segmentation function and Ω is the image domain. This ensures accurate segmentation, even for complex structures. Such methods were effectively employed in prior studies, including Soomro et al. (2023), which highlights the integration of region and edge-based functions to achieve accurate and reliable segmentation outcomes in challenging scenarios.

Finally, the geometric properties of each pore are computed. The area A and equivalent diameter β (a parameter to simplify the pore-size analysis) are defined as $\beta = 2(\pi)^{\frac{-1}{2}}(\sum_{i,j} B(i,j))^{\frac{1}{2}}$. Pores are classified into three categories in the 25 μm image shot based on β: small ($0 < \beta < 2\,\mu m$), medium ($2 < \beta < 5\,\mu m$) and large ($\beta > 5\,\mu m$).

3.2 Proposed Sound-Absorption Prediction Algorithm

The fuzzy logic-based prediction algorithm is a computational framework designed to estimate the sound absorption rate of materials. As depicted in Fig. 3, the algorithm is structured into three distinct fuzzy logic prediction engines: (a) pore size count, (b) excitation frequency, and (c) material characteristics. Each engine processes specific input parameters independently and generates individual predictions. These outputs are subsequently averaged to produce a comprehensive and accurate estimate of the overall sound absorption coefficient.
Each fuzzy logic engine incorporates three fundamental components Dernoncourt (2013):

1. Fuzzification module: This module converts crisp input values into fuzzy sets, allowing the algorithm to handle uncertainties and variations in real-world data. Inputs such as pore size counts, excitation frequency, and material characteristics (e.g., porosity, density, and thickness) are transformed into linguistic variables using membership functions.
2. Prediction engine (Inference System): Serving as the algorithm's core, this component applies a predefined set of rules stored in a rule base. These rules define how fuzzy inputs interact to generate intermediate fuzzy outputs, modelling the intricate relationships between the input parameters and the material's sound absorption behaviour. Expert knowledge embedded in the rule base guides this process.
3. Defuzzification module: In the final stage, the intermediate fuzzy outputs are converted back into crisp values, providing actionable numerical predictions for the sound absorption coefficients.

To reduce the complexity of the rule base, the algorithm is divided into three fuzzy logic engines, each focused on processing a specific set of parameters, thereby improving the computational efficiency and accuracy. Fuzzy logic, a computational approach inspired by human reasoning, incorporates the concept of "degrees of truth" rather than binary logic (true or false). Introduced by Lotfi Zadeh in 1965 Zadeh (1965), fuzzy logic was extensively applied across various fields to model complex systems characterised by uncertainty, ambiguity, or imprecise data. By using linguistic variables, membership functions, and rule-based reasoning, fuzzy logic to capable of addressing the problems that are challenging to solve with conventional mathematical methods. Its versatility made fuzzy logic a valuable tool in numerous prediction tasks. For example, Janarthanan et al. (2021) developed a fuzzy logic-based model to estimate rainfall, effectively handling uncertain environmental data. Similarly, Azmi (2012) utilised fuzzy logic to predict cutting tool performance during machining processes, demonstrating its efficacy in industrial applications. In the domain of acoustic materials, Mondal and Hussain (2023) applied fuzzy logic to predict the acoustic properties of banana-glass fibre composites, demonstrating their ability to model complex material behaviour. Collectively, these studies highlight the adaptability and effectiveness of fuzzy logic in addressing diverse prediction challenges in a variety of fields.

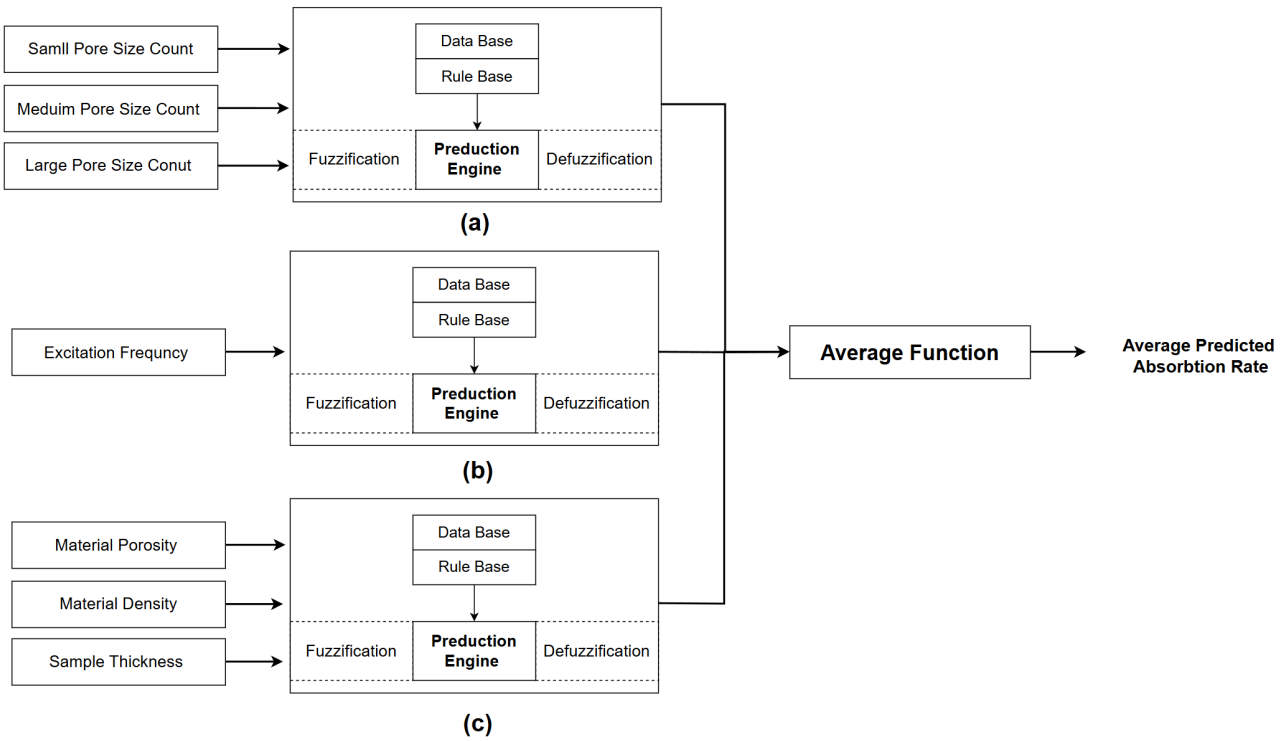

Fig. 3: Overview of the fuzzy logic prediction algorithms (a) Fuzzy logic engine for pore size count (b) Fuzzy logic engine for excitation frequency (c) Fuzzy logic engine for material characteristics

The fuzzy logic engine for pore size count:
The first fuzzy logic engine focuses on evaluating the effect of pore size count on the predicted sound absorption coefficient. As discussed in Section 2.2, the pore size distribution plays a crucial role in determining the material's acoustic performance. This engine is designed with three input membership functions: small, medium, and large pore size counts. Each input is represented using linguistic variables such as Very Low (VL), Low (L), Medium (M), High (H), and Very High (VH), and each term has a triangular membership function with parameters based on the following ranges:
The membership functions for the input variable Small_Pore_Size_Count_MF are defined as follows:

$$\mu(x) = \begin{cases} \text{Very Low (VL):} & \mu_{VL}(x) = 1 - \frac{x}{3000}, \quad 0 \le x \le 3000, \\ & \mu_{VL}(x) = 0, \quad x > 3000, \\ \text{Low (L):} & \mu_{L}(x) = \frac{x}{3000}, \quad 0 \le x \le 3000, \\ & \mu_{L}(x) = 1 - \frac{x-3000}{2000}, \quad 3000 \le x \le 5000, \\ & \mu_{L}(x) = 0, \quad \text{otherwise}, \\ \text{Medium (M):} & \mu_{M}(x) = \frac{x-3000}{2000}, \quad 3000 \le x \le 5000, \\ & \mu_{M}(x) = 1 - \frac{x-5000}{2000}, \quad 5000 \le x \le 7000, \\ & \mu_{M}(x) = 0, \quad \text{otherwise}, \\ \text{High (H):} & \mu_{H}(x) = \frac{x-5000}{2000}, \quad 5000 \le x \le 7000, \\ & \mu_{H}(x) = 1 - \frac{x-7000}{2000}, \quad 7000 \le x \le 9000, \\ & \mu_{H}(x) = 0, \quad \text{otherwise}, \\ \text{Very High (VH):} & \mu_{VH}(x) = \frac{x-7000}{3000}, \quad 7000 \le x \le 10000, \\ & \mu_{VH}(x) = 0, \quad x < 7000. \end{cases} \tag{6}$$

The structure of the membership functions for medium and large pore size counts is similar to the small pore size count membership functions. However, the range of values and breakpoints used in these membership functions are adjusted based on the results of the pore size identification algorithm discussed in Section 3.1. These ranges are determined by analysing the pore size distribution across different samples. For medium pore size count, the values typically span from 2000 to 8000, while for large pore size count, the range is extended further, often between 3000 and 10,000. The specific breakpoints are chosen to reflect the unique characteristics and clustering behaviour of pore sizes observed in each sample, ensuring accurate modelling and representation of the data within the fuzzy logic framework.
Additionally, there is one output membership function, "Condition 1," which represents the predicted contribution of pore size count to the overall sound absorption coefficient. The membership functions for the three input variables are shown in Fig. 4 (a), (b), and (c), illustrating their respective fuzzy sets. Fig. 4 (d) demonstrates the output membership function, while Fig. 4 (e) provides a 3D visualisation of the interaction between small and medium pore size counts and their impact on the output variable.
Output membership function: condition1
This variable also uses triangular membership functions distributed along the normalized range $[0, 1]$. The membership functions are defined as follows:

$$\mu(x) = \begin{cases} \text{Very Low (VL):} & 1, \quad x \le 0, \\ & \frac{0.3-x}{0.3}, \quad 0 < x \le 0.3, \\ & 0, \quad x > 0.3, \\ \text{Low (L):} & \frac{x-0}{0.3}, \quad 0 \le x < 0.3, \\ & \frac{0.6-x}{0.3}, \quad 0.3 \le x \le 0.6, \\ & 0, \quad \text{otherwise}, \\ \text{Medium (M):} & \frac{x-0.3}{0.3}, \quad 0.3 \le x < 0.6, \\ & \frac{0.9-x}{0.3}, \quad 0.6 \le x \le 0.9, \\ & 0, \quad \text{otherwise}, \\ \text{High (H):} & \frac{x-0.6}{0.3}, \quad 0.6 \le x < 0.9, \\ & \frac{1-x}{0.1}, \quad 0.9 \le x \le 1, \\ & 0, \quad \text{otherwise}, \\ \text{Very High (VH):} & \frac{x-0.9}{0.1}, \quad 0.9 \le x < 1, \\ & 1, \quad x \ge 1, \\ & 0, \quad \text{otherwise}. \end{cases} \tag{7}$$

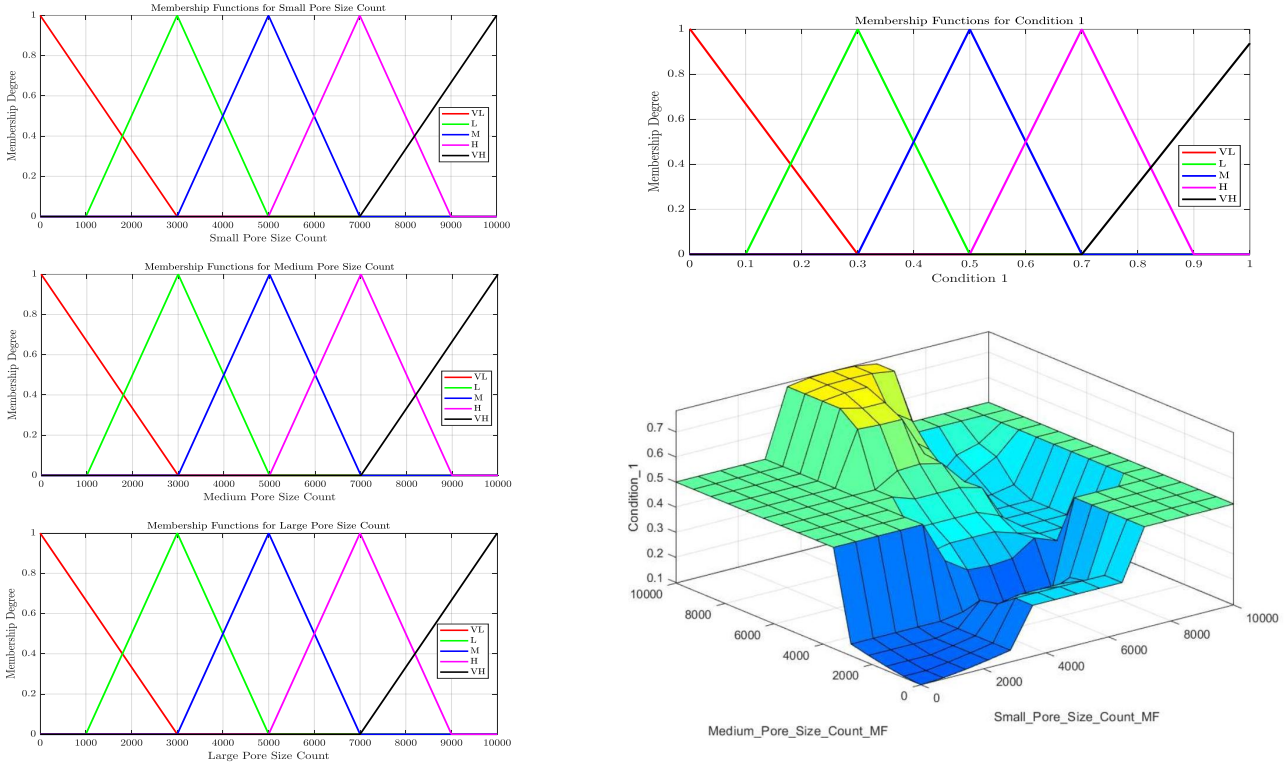

Fig. 4: Membership Functions and 3D Surface Plot of the First Fuzzy Logic Engine

The fuzzy logic engine for frequency excitation:

The second fuzzy logic engine focuses on evaluating the effect of excitation frequency on the predicted sound absorption coefficient by utilising tailored membership functions and fuzzy inference rules. Fig. 5 shows the engine input membership function: (a) input membership function plots for the variable "Excitation Acoustic Frequencies MF" and (b) output membership function plots for the variable "Condition 2," illustrating fuzzy sets for different conditions. (d) The resulting 2D surface curve depicts the fuzzy inference system's output, "Condition 2," as a function of the input excitation acoustic frequencies.

Membership functions for excitation acoustic frequencies: The membership functions (Very Low (VL), Low (L), Medium (M), High (H), Very High (VH)) are distributed along the range $[0, 1600]$ Hz. Assuming linear transitions, the parameters for each

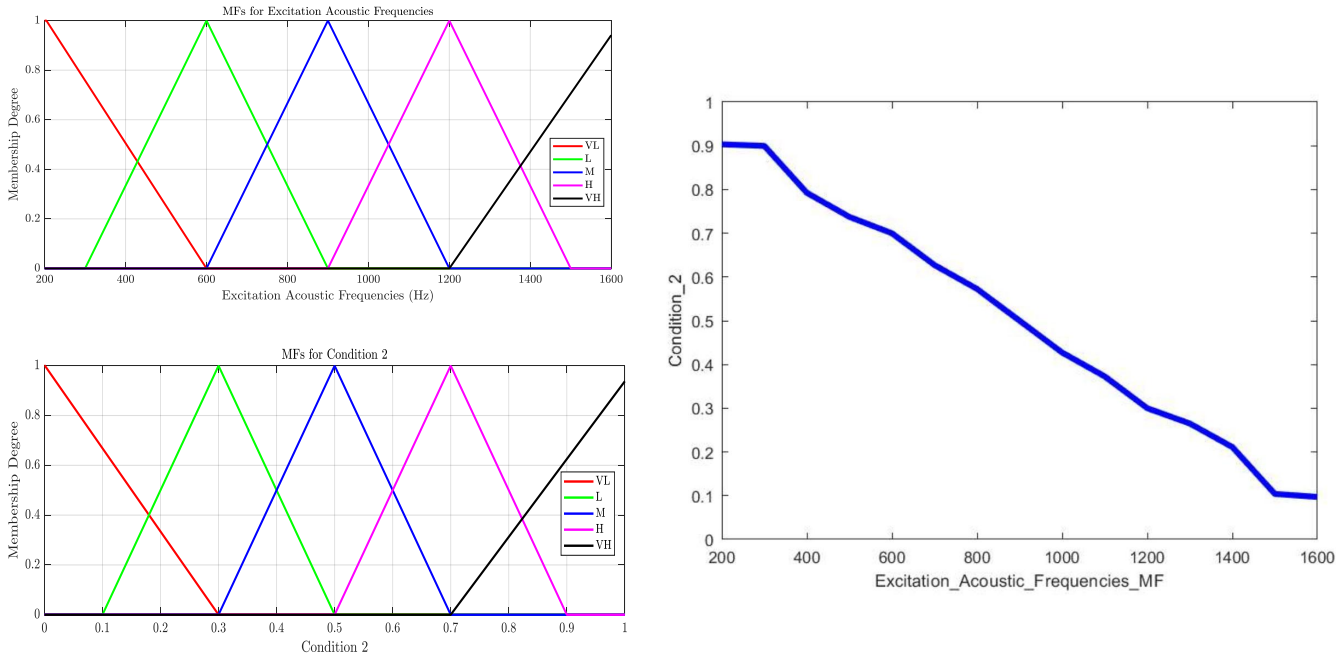

Fig. 5: Membership Functions and 2D Surface Plot of the Second Fuzzy Logic Engine

triangular membership function (MF) are defined as follows:

$$\mu(x) = \begin{cases} \text{Very Low (VL):} & 1, \quad x \leq 0, \\ & \frac{400-x}{400}, \quad 0 < x \leq 400, \\ & 0, \quad x > 400, \\ \text{Low (L):} & \frac{x-0}{400}, \quad 0 \leq x < 400, \\ & \frac{800-x}{400}, \quad 400 \leq x \leq 800, \\ & 0, \quad \text{otherwise}, \\ \text{Medium (M):} & \frac{x-400}{400}, \quad 400 \leq x < 800, \\ & \frac{1200-x}{400}, \quad 800 \leq x \leq 1200, \\ & 0, \quad \text{otherwise}, \\ \text{High (H):} & \frac{x-800}{400}, \quad 800 \leq x < 1200, \\ & \frac{1600-x}{400}, \quad 1200 \leq x \leq 1600, \\ & 0, \quad \text{otherwise}, \\ \text{Very High (VH):} & \frac{x-1200}{400}, \quad 1200 \leq x < 1600, \\ & 1, \quad x \geq 1600, \\ & 0, \quad \text{otherwise}. \end{cases} \tag{8}$$

Additionally, there is one output membership function, Condition 2, which represents the predicted contribution of the excitation frequency to the overall sound absorption coefficient. This output membership function has a structure that is similar to the Condition 1 membership function from the first fuzzy logic engine, ensuring consistency across the fuzzy inference systems in this study.
The similarities between the Condition 2 and Condition 1 membership functions are intentional, as they aim to maintain a standardised linguistic and computational framework for evaluating both excitation-related parameters and their acoustic outcomes. This structural alignment ensures a unified interpretation of the fuzzy logic outputs and facilitates easier comparison between the two fuzzy logic engines.

The fuzzy logic engine for material characteristics: The third fuzzy logic engine developed for evaluating material characteristics integrates three key input parameters: material porosity (MF), material density (MF), and material thickness (MF). These input variables directly influence the acoustic absorption rate of insulation panels and are mapped to an output condition (condition 3) with corresponding membership functions (MFs). The ranges and shapes of these functions are designed to reflect the practical and physical properties of materials relevant to the insulation panel application. Fig. 6 illustrates the membership functions for the inputs and the resulting output condition.
Material Porosity (MF) denoted as P, is measured as a percentage ($0\% \leq P \leq 100\%$) and is modelled using triangular membership functions (Fig. 6 (a)). Porosity is classified into five linguistic categories: Very Low (VL), Low (L), Medium (M), High (H), and Very High (VH).
The membership function for porosity (μ_P) is mathematically defined as:

$$\mu_{P,\mathrm{VL}}(P) = \begin{cases} 1 - \frac{P}{20}, & 0 \leq P \leq 20 \\ 0, & \text{otherwise} \end{cases}, \quad \mu_{P,\mathrm{L}}(P) = \begin{cases} \frac{P-10}{20}, & 10 \leq P \leq 30 \\ 1 - \frac{P-30}{20}, & 30 \leq P \leq 50 \\ 0, & \text{otherwise} \end{cases} \tag{9}$$

Similar equations can be derived for Medium, High, and Very High based on their respective boundaries.
The range ($0\% - 100\%$) reflects the practical porosity levels observed in common acoustic insulation materials. Porosity impacts the material's ability to absorb sound, as higher porosity allows sound waves to penetrate and dissipate energy as mentioned in section 2.2.
Material Density (MF) denoted as D, is measured in $\mathrm{kg/m^3}$ within the range $0\,\mathrm{kg/m^3} \leq D \leq 700\,\mathrm{kg/m^3}$ and categorized into five linguistic terms: Very Low (VL), Low (L), Medium (M), High (H), and Very High (VH). The triangular membership functions are shown in Fig. 6 (b).
The membership function for density (μ_D) is expressed as:

$$\mu_{D,\mathrm{VL}}(D) = \begin{cases} 1 - \frac{D}{140}, & 0 \leq D \leq 140 \\ 0, & \text{otherwise} \end{cases}, \quad \mu_{D,\mathrm{L}}(D) = \begin{cases} \frac{D-70}{140}, & 70 \leq D \leq 210 \\ 1 - \frac{D-210}{140}, & 210 \leq D \leq 350 \\ 0, & \text{otherwise} \end{cases} \tag{10}$$

Other membership functions for higher density levels follow similar patterns.

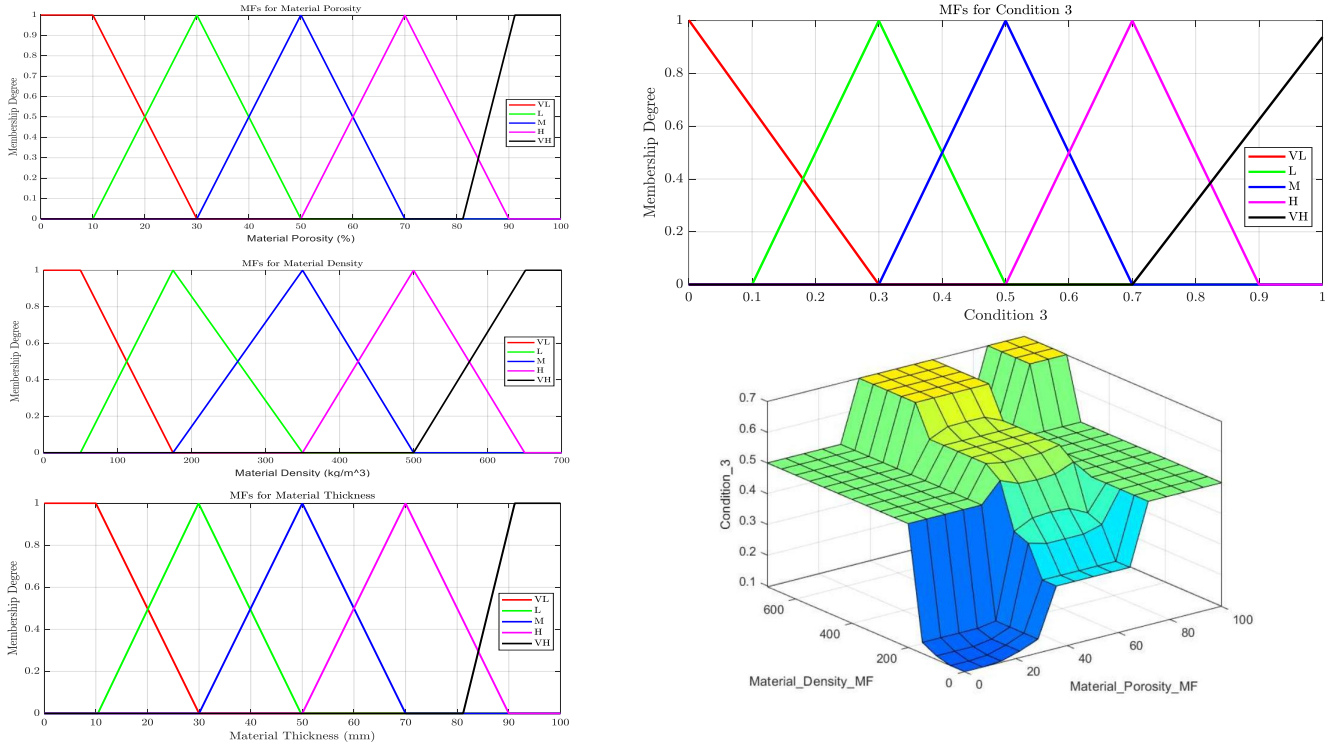

Fig. 6: Membership Functions and 3D Surface Plot of the Third Fuzzy Logic Engine

This range was chosen based on the density values of commonly used insulation materials, such as foams and fibres. Lower densities are associated with better sound absorption at high frequencies, while higher densities enhance low-frequency sound insulation due to the mass law effect.

Material Thickness (MF) denoted as T, ranges from $0\,\text{mm} \leq T \leq 100\,\text{mm}$ and is divided into five linguistic categories: Very Low (VL), Low (L), Medium (M), High (H), and Very High (VH). The membership functions for thickness are presented in Fig. 6 (c).

The membership function for thickness (μ_T) is defined as:

$$\mu_{T,\text{VL}}(T) = \begin{cases} 1 - \frac{T}{20}, & 0 \leq T \leq 20 \\ 0, & \text{otherwise} \end{cases}, \quad \mu_{T,\text{L}}(T) = \begin{cases} \frac{T-10}{20}, & 10 \leq T \leq 30 \\ 1 - \frac{T-30}{20}, & 30 \leq T \leq 50 \\ 0, & \text{otherwise} \end{cases} \tag{11}$$

Higher thickness levels follow a similar pattern.

The range ($0-100\,\text{mm}$) was selected to encompass typical insulation panel thicknesses used in residential and industrial applications. Increased thickness improves sound absorption, especially at lower frequencies, due to the increased interaction of sound waves with the material.

Output condition (Condition 3) maps the combined effects of porosity, density, and thickness to an aggregated output range ($0 \leq C_3 \leq 1$) using five linguistic terms: Very Low (VL), Low (L), Medium (M), High (H), and Very High (VH) as condition 1 and condition 2. The output membership functions are shown in Fig. 6 (d).

The interaction of the inputs is visualized in a three-dimensional surface plot (Fig. 6(e)), which demonstrates the non-linear relationship between the input parameters and the resulting acoustic performance.

4 Results and Discussion

The performance of the proposed fuzzy logic-based prediction algorithm for sound absorption coefficients was validated by conducting a series of experiments on a polymer composite using an impedance tube, following the ISO 10534-2 standard. This section presents a comprehensive analysis of the experimental results, comparing them with the predicted values generated by the algorithm. Three different composite masses are coffee-chaff-based, with a 10 cm diameter, and were prepared, weighing 100 g, 80 g, and 50 g, respectively. The sound absorption coefficient was measured across a frequency range from 200 to 1600 Hz using an impedance-tube setup shown in Fig. 7. The experimental results for the three composite samples are presented in Fig. 8.

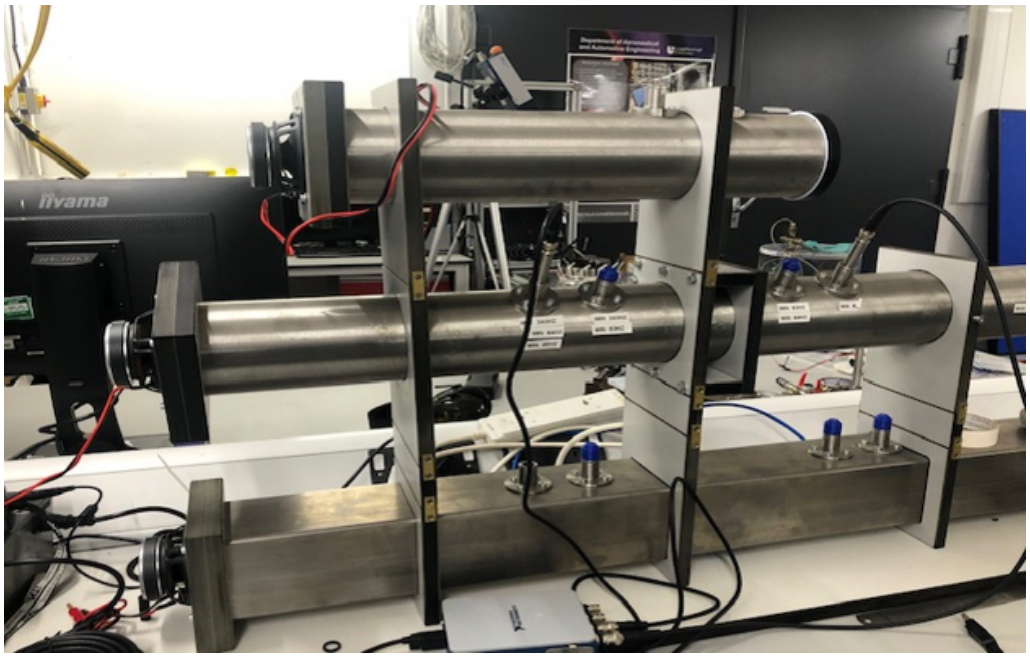

Fig. 7: (a) ISO 10534-2 impedance-tube experimental setup.

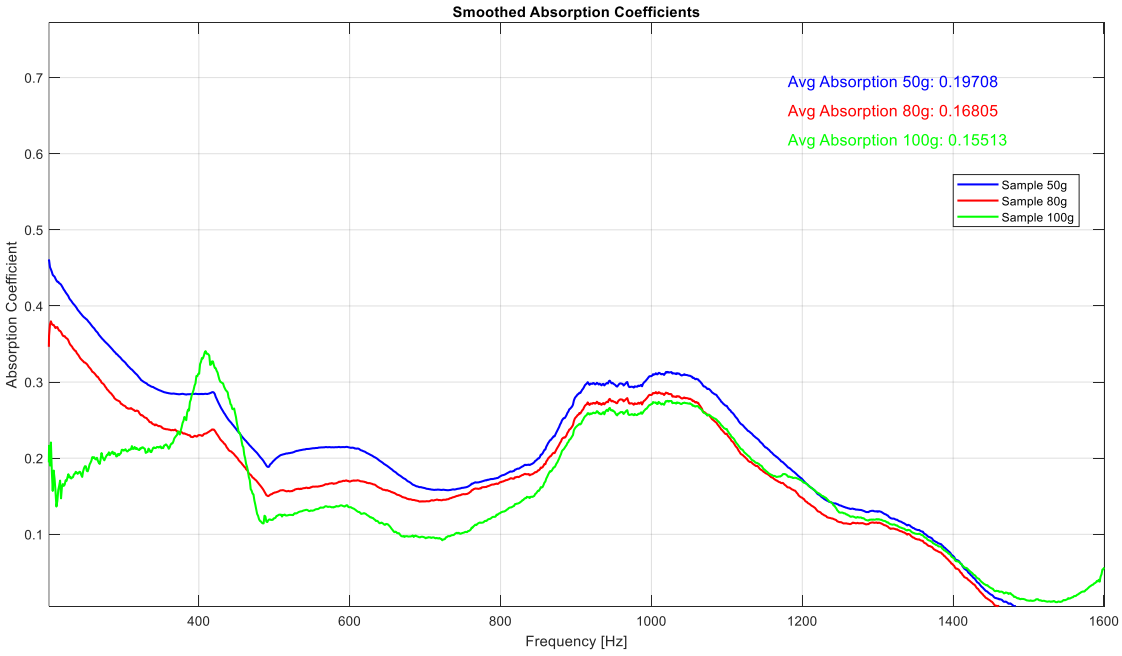

Fig. 8: Experimental results for three composite samples.

The absorption coefficient for each sample was calculated and compared with the corresponding values predicted with the fuzzy-logic algorithm. Tab. 1 provides a comparison between the experimental results and the predicted data.

Experimental Results		**Predicted Data**	
200 – 1600 Hz		200 – 1600 Hz	
Samples (g)	**Experimental absorption coefficient**	**Predicted absorption coefficient**	**Prediction Error (%)**
100 g	0.1513	0.1938	28.1
80 g	0.16.80	0.1858	10.6
50 g	0.1970	0.2367	20.2

Tab. 1: Comparison of experimental and predicted absorption coefficients.

The experimental results illustrate the efficacy of the fuzzy logic-based prediction algorithm in estimating the sound absorption rate

for different composite material samples, as evidenced by its reasonable level of accuracy, with the highest absolute error 28.1% for the 100 g sample. This indicates that the algorithm is robust and effective in accounting for variations in material properties such as density, porosity, and sample thickness. However, some discrepancies between the experimental and predicted values, particularly for the heavier sample, highlight the complexities inherent in the material structure and the interactions between various influencing factors, including pore size distribution and acoustic resonance effects. The anomalies observed, such as the discontinuity in the absorption coefficient graph near 400 Hz, emphasize the importance of understanding these interactions. This dip, most pronounced in the 80 g and 100 g samples, can be attributed to resonance effects resulting from the interaction of sound waves with the composites' internal structure, such as its density variations and non-uniform pore distribution. These resonance effects are characteristic of porous materials, where specific frequencies can induce localized behaviours that reduce sound absorption efficiency. In particular, the 50 g sample consistently exhibits higher absorption in this frequency range, likely due to its lower density and greater sound wave penetration. This leads to more effective interaction with the material's microstructure. This finding underscores the influence of density and porosity in determining the acoustic properties of the samples. Additionally, these anomalies could reflect limitations in the algorithm's current fuzzy logic rule base, which, while effective, may not fully encapsulate the complexities of the heavier samples' structural heterogeneity. Enhancing the algorithm's performance might involve expanding the fuzzy logic rules or integrating additional parameters to capture the nuances of material behaviour more accurately. Parameters such as pore connectivity, tortuosity, and specific acoustic impedance could be included to model the interactions between structural factors and sound waves in greater detail.

The observed discrepancies, especially at particular frequencies, i.e., 400 Hz, could also be linked to transitions in the material's acoustic response, where shifts in absorption behaviour may be influenced by local resonances within the composite. These resonances are determined by the interplay of pore geometry, size distribution, and material density, all of which affect the propagation and dissipation of sound energy. By incorporating more detailed mathematical relationships between the pore size and the acoustic parameters, the fuzzy logic algorithm could better simulate these effects and reduce prediction errors. Furthermore, adding experimental data from broader sample ranges or varying structural configurations might help refine the algorithm's predictive capacity, ensuring accuracy across diverse scenarios. The results further validate the importance of correlating fuzzy-logic-based predictions with experimental findings to identify and address potential shortcomings in the algorithm. For instance, while the algorithm effectively accounts for average trends in sound absorption performance, its sensitivity to discontinuities and localized anomalies could be enhanced through iterative refinements. One approach could involve adjusting the membership functions and rule definitions to better align with the observed experimental data, particularly for heavier and denser samples. Similarly, conducting a more detailed investigation of the pore-size distribution, particularly contributions of medium and small pores, could help isolate and address the underlying causes of discrepancies between predicted and experimental values.

The proposed fuzzy logic-based image analysis algorithm prediction method offers a cost-effective and efficient alternative to the traditional impedance tube approach to predict acoustic performance. A typical impedance-tube setup, including microphones, a high-frequency data acquisition card, and calibration equipment, costs $5,000–$10,000, with additional annual maintenance expenses of $500–$1,000, as reported in similar acoustic-measurement studies Deshpande and Rao (2014) Instruments (2024). In contrast, the proposed method requires only a high-resolution microscope and basic laboratory equipment, with an estimated one-time cost of $1,000 to $2,000. This results in potential cost savings of up to 80%, in addition to faster data acquisition and reduced labour requirements. Unlike impedance tube measurements, which are time-intensive and require multiple prepared samples, the proposed method provides flexibility, allowing the analysis of various material configurations without extensive physical tests. This further increases its practicality and accessibility for laboratories with limited budgets. These advantages, combined with the adaptability of the algorithm to various material properties, demonstrate its potential as a transformative tool in acoustic analysis.

5 Conclusion

The study presents an innovative predictive framework for determining the acoustic coefficients of sound insulation panels by leveraging fuzzy logic techniques and high-resolution microscopic image analysis. By focusing on the microscopic structural properties of materials, the proposed algorithm delivers accurate predictions of sound absorption coefficients, providing a cost-effective and time-efficient alternative to conventional experimental methods. High-resolution imaging and advanced processing techniques enable the algorithm to analyse critical material characteristics, such as porosity and density, ensuring reliable and consistent acoustic performance predictions. Experimental validation confirms the robustness of the approach, with prediction errors remaining within acceptable limits across various material samples. These findings highlight the practicality and industrial significance of the algorithm for acoustics engineers and material scientists. Despite its strengths, the study acknowledges some limitations, particularly the complex interactions within the material microstructure, which can lead to minor discrepancies between predicted and experimental results. While the predictive framework is robust, addressing these complexities could further enhance its accuracy and broaden its applicability to a wider range of material systems. Building on this foundation, future work could focus on incorporating additional parameters, such as anisotropic material behaviour, non-linear acoustic effects, or temperature dependencies, to refine the predictive model further. Integrating these factors into the fuzzy logic rules would enable the algorithm to handle more complex and heterogeneous materials with greater precision. Additionally, expanding the approach to include multi-scale modelling—combining microscopic and macroscopic analyses—could offer a more comprehensive understanding of material behaviour under real-world conditions. Further experimental validation under diverse environmental conditions, such as varying humidity and temperature, would enhance the model's reliability and applicability across a broader range of operational scenarios. Exploring more complex material systems, such as composite or hybrid materials, could also extend the predictive framework's utility. Furthermore, integrating machine learning techniques with fuzzy logic could facilitate

adaptive rule refinement, improving the algorithm's capacity to generalise across new materials and acoustic environments. This integration could lead to more robust predictions and enable the model to evolve alongside advancements in material science. By harnessing the strengths of both machine learning and fuzzy logic, researchers could develop systems that not only predict behaviour accurately but also adapt dynamically to changing conditions and novel material properties.

References

Mohsen Aliabadi, Rostam Golmohammadi, Abdolreza Ohadi, Muharram Mansoorizadeh, Hassan Khotanlou, and Mohammad Saber Sarrafzadeh. Development of an empirical acoustic model for predicting reverberation time in typical industrial workrooms using artificial neural networks. *Acta Acustica united with Acustica*, 100(6):1090–1097, 2014.

Kannan Allampalayam Jayaraman et al. Acoustical absorptive properties of nonwovens. *Fiber Innovation Technology, Inc.*, 2005.

B Arunkumar and S Jeyanthi. Design and analysis of impedance tube for sound absorption measurement. *ARPN J Eng Appl Sci*, 12(5):1400–5, 2017.

Sadao Aso and Rikuhiro Kinoshita. Maximum sound absorption coefficient of a fiber assembly. *Journal of the Textile Machinery Society of Japan*, 11(3):81–87, 1965.

Standard Test Method for Impedance and Absorption of Acoustical Materials Using a Tube, Two Microphones and a Digital Frequency Analysis System. ASTM International, West Conshohocken, PA, USA, 2012. URL https://doi.org/10.1520/E1050-12. ASTM E1050-12.

Standard Test Method for Normal Incident Determination of Porous Material Acoustical Properties Based on the Transfer Matrix Method. ASTM International, West Conshohocken, PA, USA, 2017. URL https://doi.org/10.1520/E2611-17. ASTM E2611-17.

A.I. Azmi. Design of fuzzy logic model for the prediction of tool performance during machining of composite materials. *Procedia Engineering*, 38:208–217, 2012. ISSN 1877-7058. doi: https://doi.org/10.1016/j.proeng.2012.06.028. URL https://www.sciencedirect.com/science/article/pii/S1877705812019418. INTERNATIONAL CONFERENCE ON MODELLING OPTIMIZATION AND COMPUTING.

David A Bies, Colin H Hansen, and Carl Q Howard. *Engineering noise control*. CRC press, 2017.

Tatiana Budtova, Tapio Lokki, Sadeq Malakooti, Ameya Rege, Hongbing Lu, Barbara Milow, Jaana Vapaavuori, and Stephanie Vivod. Acoustic properties of aerogels: current status and prospects. *Advanced Engineering Materials*, 25(6):2201137, 2023.

Bernard Castagnède, Achour Aknine, Bruno Brouard, and Viggo Tarnow. Effects of compression on the sound absorption of fibrous materials. *Applied Acoustics*, 61(2):173–182, 2000. ISSN 0003-682X. doi: https://doi.org/10.1016/S0003-682X(00)00003-7. URL https://www.sciencedirect.com/science/article/pii/S0003682X00000037.

Franck Dernoncourt. Introduction to fuzzy logic. *Massachusetts Institute of Technology*, 21:50–56, 2013.

Satyajeet P Deshpande and Mohan D Rao. Development of a low-cost impedance tube to measure acoustic absorption and transmission loss of materials. In *2014 ASEE Annual Conference & Exposition*, pages 24–417, 2014.

Masataka Hakamada, Tetsunume Kuromura, Youqing Chen, Hiromu Kusuda, and Mamoru Mabuchi. Sound absorption characteristics of porous aluminum fabricated by spacer method. *Journal of Applied Physics*, 100(11), 2006.

Nandeesh Hiremath, Vaibhav Kumar, Nicholas Motahari, and Dhwanil Shukla. An overview of acoustic impedance measurement techniques and future prospects. *Metrology*, 1(1):17–38, 2021.

Andreas Höpe. Diffuse reflectance and transmittance. In *Experimental Methods in the Physical Sciences*, volume 46, pages 179–219. Elsevier, 2014.

Carl Hopkins. *Sound insulation*. Routledge, 2012.

ROGA Instruments. Impedance tubes, 2024. URL https://roga-instruments.com/impedance-tubes/. Accessed: 2024-11-22.

Acoustics – Determination of sound absorption coefficient and impedance in impedance tubes – Part 2: Transfer-function method. International Organization for Standardization, Geneva, Switzerland, 2002. ISO 10534-2:1998.

Acoustics – Laboratory measurement of sound insulation of building elements. Part 2: Measurement of airborne sound insulation. International Organization for Standardization, Geneva, Switzerland, 2010. ISO 10140-2.

Acoustics – Measurement of sound absorption in a reverberation room. International Organization for Standardization, Geneva, Switzerland, 2015. ISO 354:2003.

R. Janarthanan, R. Balamurali, A. Annapoorani, and V. Vimala. Prediction of rainfall using fuzzy logic. *Materials Today: Proceedings*, 37:959–963, 2021. ISSN 2214-7853. doi: https://doi.org/10.1016/j.matpr.2020.06.179. URL https://www.sciencedirect.com/science/article/pii/S2214785320346332. International Conference on Newer Trends and Innovation in Mechanical Engineering: Materials Science.

Douglas H Keefe, Robert Ling, and Jay C Bulen. Method to measure acoustic impedance and reflection coefficient. *The Journal of the Acoustical Society of America*, 91(1):470–485, 1992.

Yang-Hann Kim. *Sound propagation: an impedance based approach*. John Wiley & Sons, 2010.

Cheuk Ming Mak and Zhen Wang. Recent advances in building acoustics: An overview of prediction methods and their applications. *Building and Environment*, 91:118–126, 2015. ISSN 0360-1323.

A Maria, J Kuczmarski, and C Johnston. Acoustic absorption in porous materials. *NASA/TM*, 216995, 2011.

Moni Sankar Mondal and Syed Zubair Hussain. Banana-glass fiber composite for acoustic insulation and prediction of its properties by fuzzy logic system. *Journal of Natural Fibers*, 20(2):2212928, 2023.

Anthony Nash. Qualification of an anechoic chamber. In *Proceedings of the 23rd International Congress on Acoustics (ICA 2019)*, Aachen, Germany, 2019.

L. Peng. 13 - sound absorption and insulation functional composites. In Mizi Fan and Feng Fu, editors, *Advanced High Strength Natural Fibre Composites in Construction*, pages 333–373. Woodhead Publishing, 2017. ISBN 978-0-08-100411-1. doi: https://doi.org/10.1016/B978-0-08-100411-1.00013-3. URL https://www.sciencedirect.com/science/article/pii/B9780081004111000133.

Arash Rabbani, Saeid Jamshidi, and Saeed Salehi. *Pore size distribution of 2D porous media images*. MATLAB, 2014. URL https://uk.mathworks.com/matlabcentral/fileexchange/50623-pore-size-distribution-of-2d-porous-media-images?s_tid=prof_contriblnk.

Jinbao Shao, Yuexiao Lv, Zhenhua Xue, Yanfei Pan, Jinwei Liu, Mayin Dai, and Fengqi Qiu. Preparation and acoustic performance of porous aerogel composites of graphene oxide and cellulose. *Coatings*, 14(4):441, 2024.

Shafiullah Soomro, Asim Niaz, Toufique Ahmed Soomro, Jin Kim, Adnan Manzoor, and Kwang Nam Choi. Selective image segmentation driven by region, edge and saliency functions. *Plos one*, 18(12):e0294789, 2023.

Douglas Thorby. *Structural dynamics and vibration in practice: an engineering handbook*. Butterworth-Heinemann, 2008.

Michael Vorländer. Building acoustics: From prediction models to auralization. In *Proceedings of Acoustics*, volume 20, pages 11–22, 2006.

Lotfi A Zadeh. Fuzzy sets. *Information and Control*, 1965.

Yong-Bin Zhang, Wang-Lin Lin, and Chuan-Xing Bi. A technique based on the equivalent source method for measuring the surface impedance and reflection coefficient of a locally reacting material. In *INTER-NOISE and NOISE-CON Congress and Conference Proceedings*, volume 249, pages 3220–3227. Institute of Noise Control Engineering, 2014.